Size Effect on Strength of Quasibrittle Structures with Reentrant Corners Symmetrically Loaded in Tension

Zdeněk P. Bažant[1] and Qiang Yu[2]

Abstract: The effect of V-notches (or reentrant corners) on fracture propagation has been analyzed for brittle materials, but not for quasibrittle materials such as concrete, marked by a large material characteristic length producing a strong size effect transitional between plasticity and linear elastic fracture mechanics. A simple size effect law for the nominal strength of quasibrittle structures with symmetrically loaded notches, incorporating the effect of notch angle, is derived by asymptotic matching of the following five limit cases: (1) Bažant's size effect law for quasibrittle structures with large cracks for notch angle approaching zero; (2) absence of size effect for vanishing structure size; (3) absence of size effect for notch angle approaching π; (4) plasticity-based notch angle effect for vanishing size; and (5) the notch angle effect on crack initiation in brittle structures, which represents the large-size limit of quasibrittle structures. Accuracy for the brittle large-size limit, with notch angle effect only, is first verified by extensive finite-element analyses of bodies with various notch angles. Then a cohesive crack characterized by a softening stress-separation law is considered to emanate from the notch tip, and the same finite-element model is used to verify and calibrate the proposed law for size and angle effects in the transitional size range in which the body is not far larger than Irwin's material characteristic length. Experimental verification of the notch angle effect is obtained by comparisons with Dunn et al.'s extensive tests of three-point-bend notched beams made of plexiglass (polymethyl methacrylate), and Seweryn's tests of double-edge-notched tension specimens, one set made of plexiglass and another of aluminum alloy.

DOI: 10.1061/(ASCE)0733-9399(2006)132:11(1168)

CE Database subject headings: Size effect; Fracture; Concrete; Notches; Stress concentration.

Introduction

In contrast to brittle metals, V-notches (or sharp reentrant corners) have generally been perceived as innocuous for quasibrittle materials such as concrete. This perception, however, is correct only on small enough scale—for cross section sizes less than about 20 times the dominant material inhomogeneities, which is about 0.5 m for ordinary concrete structures (but not for huge concrete structures such as the record-span prestressed box girder in Palau, which had cross section depth 14.2 m and collapsed with fracture emanating from a sharp corner at the junction of the pier and the box girder). When the cross section becomes more than 100 times larger than the maximum size of material inhomogeneities (the aggregate pieces in concrete), a quasibrittle structure behaves as perfectly brittle and thus must be notch sensitive, exhibiting size effect.

Although the size effect for V-notches is automatically captured by the nonlocal or crack-band finite-element models based on nonlinear fracture mechanics, its analytical description, particularly the effect of notch angle, is unavailable. Determining this effect is the objective of this paper, expanding a recent brief conference presentation (Bažant and Yu 2004).

Among the solutions of the singular elastic stress field at V-notches (Knein 1926, 1927; Brahtz 1933; Williams 1952; Karp and Karal 1962; England 1971), we adopt as the point of departure Williams' solution based on Airy stress function, which is applicable to any combination of free and fixed notch faces [for an extension to fixed-sliding faces, see Kalandiia (1969)]. The effect of corners and notches on triggering brittle fracture has been analyzed by Ritchie et al. (1973) and Kosai et al. (1993), who used McClintock's (1958) criterion according to which the crack propagates when the stress at a certain distance from notch tip, proportional to Irwin (1958) characteristic material length l_0, reaches the material tensile strength. This criterion will be applied here for the brittle asymptotic case of size effect. Carpinteri (1987) and Dunn et al. (1996) assumed fracture to propagate from notch tip when a certain critical value is reached by the critical generalized stress intensity factor, K_γ, having the nonstandard physical dimension of N $m^{-1-\lambda}$, where λ = stress singularity exponent, $0.5 \leqslant \lambda \leqslant 1$. Although this criterion lacks physical meaning (because, unlike the square of stress intensity factor K_I for cracks, K_γ^2 has nothing to do with the energy release rate), Carpinteri, Dunn et al., and Gómez and Elices (2003) found good agreement with tests on brittle materials following linear elastic fracture mechanics (LEFM). Gómez and Elices' work, as well as the present analysis, shows that the use of K_γ is supported by the cohesive crack model (to avoid the awkward physical dimension, Gómez and Elices proposed replacing K_γ with dimensionless $K^* = l_0^{\lambda-1/2} K_\gamma / K_I$). A modification of Griffith's (1920) energy release rate criterion for mixed-mode cracks and V-notches was

[1]McCormick Institute Professor and W. P. Murphy Professor of Civil Engineering and Materials Science, Northwestern Univ., 2145 Sheridan Rd., CEE, Evanston, IL 60208 (corresponding author). E-mail: z-bazant@northwestern.edu

[2]Graduate Research Assistant and Doctoral Candidate, Northwestern Univ., Evanston, IL 60208. E-mail: qiangyu@northwestern.edu

Note. Associate Editor: Yunping Xi. Discussion open until April 1, 2007. Separate discussions must be submitted for individual papers. To extend the closing date by one month, a written request must be filed with the ASCE Managing Editor. The manuscript for this paper was submitted for review and possible publication on July 18, 2005; approved on March 3, 2006. This paper is part of the ***Journal of Engineering Mechanics***, Vol. 132, No. 11, November 1, 2006. ©ASCE, ISSN 0733-9399/2006/11-1168–1176/$25.00.

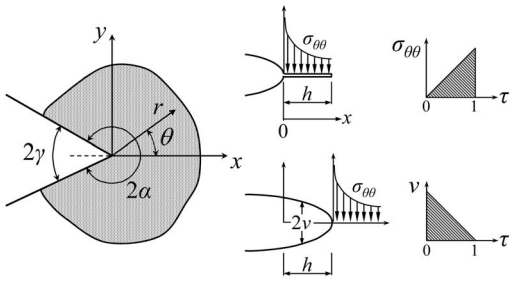

Fig. 1. (Left) Geometry of angular notch and coordinate system; (middle) stress and displacement distributions along crack line before and after crack advance by h; and (right) variation of their parameter

proposed by Palaniswamy and Knauss (1972), Hussain et al. (1974), and Wang (1978). Novožilov (1969) and Seweryn and Mróz (1995) introduced a nonlocal criterion in which the brittle fracture criterion is averaged over a zone of a certain fixed length ahead of the tip.

General Nature of Near-Tip Singularities

Consider a two-dimensional body with a sharp V-notch (Fig. 1), and let the origin of polar coordinates (r,θ) be placed into the tip. If the body is infinite, it must be a self-similar problem, and so the solution must have the separated form: $f(r,\theta)=r^{\lambda}\Phi(\theta)$. Then the stress field is given by: $\sigma_{ij}=r^{\lambda-1}f_{ij}(\theta)$, where $f_{ij}(\theta)$=functions of θ, and λ playing the role of an eigenvalue. For V-notches, the smallest $\lambda-1<0$, and so $\sigma_{ij},\epsilon_{ij}\to\infty$ for $r\to 0$. This field was derived by Knein (1926, 1927) who rejected its singularity and mistakenly used only the nonsingular fields for higher (positive) eigenvalues. However, only a singular stress field of exponent $-1/2$ can convey a nonzero energy flux into the fracture process zone (FPZ) (Bažant and Estenssoro 1979). This may be proven as follows, even without knowing the angular dependence.

Because elasticity is path independent, we may imagine a sudden infinitely small advance of the crack tip from $x=0$ to h while the stress and displacement fields are frozen (see Fig. 1). This creates on infinitesimal segment $(0,h)$ nonequilibrium profiles of normal stress $\sigma=\sigma_{22}=Ax^{\lambda-1}$ and crack-opening displacement $v=u_2=B(h-x)^{\lambda}$ (A,B=constants). To regain equilibrium, these profiles are then gradually varied as $\sigma=(1-\tau)Ax^{\lambda-1}$ and $u_2=v=\tau B(h-x)^{\lambda}$ where τ=parameter varying from 0 to 1. The flux of energy into the advancing crack tip may be calculated from the work of σ on v

$$\mathcal{E}=\lim_{h\to 0}\frac{1}{h}\int_{x=0}^{h}\int_{v'=0}^{v}\sigma\,dv'\,dx$$
$$=\lim_{h\to 0}\frac{AB}{h}\int_{x=0}^{h}\int_{\tau=0}^{1}(1-\tau)x^{\lambda-1}(h-x)^{\lambda}\,d\tau\,dx$$
$$=\frac{ABI}{2}\lim_{h\to 0}h^{2\lambda-1} \tag{1}$$

where we made the substitution $x=h\xi$ and denoted $\int_0^1\xi^{\lambda-1}(1-\xi)^{\lambda}d\xi=I$. Since integral I is positive and finite for any positive λ, the flux can be finite if and only if $2\lambda-1=0$ [or $\mathrm{Re}(2\lambda-1)=0$ if eigenvalue λ is complex]. Hence, $\lambda-1=-1/2$, regardless of the angular variation of stress field [the same general conclusion was reached by Bažant and Estenssoro (1979) via the J integral].

Review of Singular Elastic Field near Notch Tip

The notch faces (Fig. 1) are traction free, given by radial rays $\theta=\pm\alpha$ where $\alpha=\pi-\gamma$. The body is elastic and isotropic, and only loadings and responses symmetric to the notch axis are considered. In view of the preceding analysis, the Airy stress function near the tip must have the form: $\phi=\phi(\theta,r)=r^{\lambda+1}F(\theta)$. If $\lambda\neq -1,0,1$ (Williams 1952)

$$F(\theta)=C_1\sin(\lambda+1)\theta+C_2\cos(\lambda+1)\theta+C_3\sin(\lambda-1)\theta+C_4\cos(\lambda-1)\theta \tag{2}$$

$$\sigma_{rr}=r^{\lambda-1}[(\lambda+1)F(\theta)+F''(\theta)] \tag{3}$$

$$\sigma_{\theta\theta}=r^{\lambda-1}\lambda(\lambda+1)F(\theta) \tag{4}$$

$$\sigma_{r\theta}=-r^{\lambda-1}\lambda F'(\theta) \tag{5}$$

$$2\mu u_r=r^{\lambda}[-(\lambda+1)F(\theta)+(1-\nu)\chi'(\theta)] \tag{6}$$

$$2\mu u_{\theta}=r^{\lambda}[-F'(\theta)+(1-\nu)(\lambda-1)\chi(\theta)] \tag{7}$$

$$\chi(\theta)=4[-C_3\cos(\lambda-1)\theta+C_4\sin(\lambda-1)\theta]/(\lambda-1) \tag{8}$$

Here μ=shear modulus and ν=Poisson's ratio [for plane strain, ν must be replaced by $\nu/(1+\nu)$]. Applying traction-free boundary conditions $\sigma_{\theta\theta}(r,\pm\alpha)=0$ and $\sigma_{r\theta}(r,\pm\alpha)=0$ to Eqs. (4) and (5), one gets for eigenvalue λ the transcendental equation $\lambda\sin 2\alpha+\sin 2\alpha\lambda=0$. If coefficients C_i in Eq. (2) are expressed in terms of K_γ normalized so that $\sigma_{\theta\theta}(\theta=0,\gamma=0)=K_I r^{\lambda-1}/\sqrt{2\pi}$, one gets

$$\sigma_{rr}=K_\gamma r^{\lambda-1}f_{rr}(\theta,\gamma),\quad f_{rr}(\theta,\gamma)=(\lambda+1)f(\theta,\gamma)+f''(\theta,\gamma) \tag{9}$$

$$\sigma_{\theta\theta}=K_\gamma r^{\lambda-1}f_{\theta\theta}(\theta,\gamma),\quad f_{\theta\theta}(\theta,\gamma)=\lambda(\lambda+1)f(\theta,\gamma) \tag{10}$$

$$\sigma_{r\theta}=K_\gamma r^{\lambda-1}f_{r\theta}(\theta,\gamma),\quad f_{r\theta}(\theta,\gamma)=-\lambda f'(\theta,\gamma) \tag{11}$$

where

$$f(\theta,\gamma)=\left[\cos(\lambda+1)\theta-\frac{(\lambda+1)\sin(\lambda+1)(\pi-\gamma)}{(\lambda-1)\sin(\lambda-1)(\pi-\gamma)}\cos(\lambda-1)\theta\right]\Big/\,3\sqrt{2\pi} \tag{12}$$

For $\gamma=\theta=0$, $\lambda=1/2$ and $K_\gamma=K_I$=Mode I stress intensity factor. Then the expression for $\sigma_{\theta\theta}$ must be the same as in LEFM, which yields: $f_{\theta\theta}(0,0)=1/\sqrt{2\pi}$.

Relating Cohesive Crack to Notch-Tip Singular Stress Field

A physically realistic approach requires considering the propagation of a cohesive crack from the notch tip (for a large structure, one might wish to consider a sharp LEFM crack, but this would cause difficulties due to having the crack tip singularity arbitrarily close to the notch tip singularity). The salient feature of the present analysis is that the length $2c_f$ of the FPZ of this crack

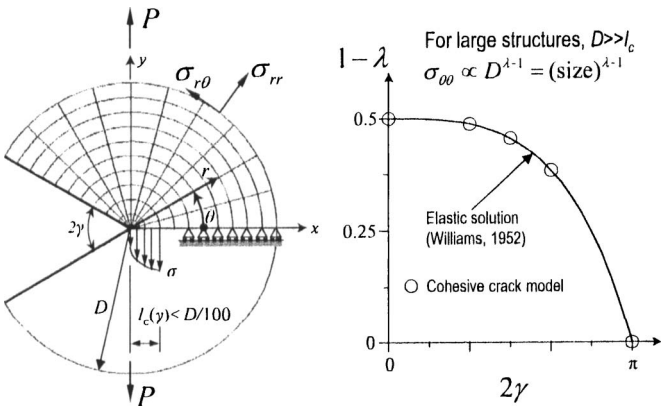

Fig. 2. (Left) Angle-notched circular specimen; (right) stress singularity exponent computed by finite elements compared to Williams' solution

must be finite, equal to l_0 times a geometry factor (Bažant and Planas 1998; Bažant et al. 2002). The FPZ must develop at the notch tip before a continuous discrete crack can propagate. In structures of positive geometry (i.e., structures in which the energy release rate at constant load is increasing with the crack length), crack propagation begins at maximum load. The cohesive crack model [developed by Barenblatt (1962) and Rice (1968), and pioneered for concrete by Hillerborg et al. (1976)] is characterized by the softening stress–separation diagram. This diagram will be here simplified as linear, which is known to suffice for predicting maximum loads. The real softening diagram for concrete is nonlinear, with a long tail, but its replacement by the initial tangent is known to suffice for predicting maximum loads (because, for positive geometries, the long tail is generally not entered prior to reaching the maximum load). The area under the linear softening diagram represents the fracture energy G_f (Rice 1968) [for nonlinear softening, G_f represents the area under the initial tangent and is called the initial fracture energy different from the total fracture energy C_F representing the area under the entire softening diagram; see e.g., Bažant et al. (2002)].

Unless the body is too small compared to the FPZ, the cohesive crack emanating from the notch tip is surrounded by the singular elastic stress field of a notch. To relate the parameters of this field to the parameters of the cohesive crack model, we consider a notched body subjected to surface tractions equal to the stresses taken from the singular elastic stress field. If the cross section of the body is sufficiently larger than the cohesive crack, various boundary shapes must lead to the same results because the same near-tip elastic field gets established farther away from the crack.

For finite-element analysis, notched bodies with circular boundaries are chosen because they are most convenient for computer programming [Fig. 2 (left)]. Condensing out the displacements of all the nodes not located on the line of the crack yields the crack compliance matrix (or discretized Green's function). The maximum loads for various notch angles 2γ and body sizes characterized by radius D of the circle have been computed using the eigenvalue method (Bažant and Li 1995a,b; Zi and Bažant 2003). This highly accurate and computationally efficient method does not necessitate step-by-step computation of the load–deflection history. Rather, one seeks directly the size D for which a given relative crack length a/D yields the maximum load ($dP/da=0$). This leads to a homogeneous Fredholm integral equation along the cohesive crack, in which D is the eigenvalue. This equation (having a nonsingular kernel) is easily solved numerically—by approximating the integral with a finite sum, which yields a matrix eigenvalue problem.

A mesh with rings of elements gradually refined as r decreases is used, except that the first 60 rings of elements near the notch tip, comprising the cohesive crack, keep the same width [see Fig. 2 (left)]. The first and second rings of elements are bounded by $r=D/6{,}000$ and $D/3{,}000$, respectively. To simulate deformations symmetric with respect to x, one must further impose at the support point on the circular boundary a prescribed displacement u_r calculated from Eq. (6) (without prescribing u_r the system would not be stable). The circular boundary is loaded by normal and tangential surface tractions equal to stresses σ_{rr} and $\sigma_{r\theta}$ taken from Williams' symmetric (Mode I) solution, as given by Eqs. (9) and (11). The resultant of these tractions in the direction normal to the symmetry axis x is denoted as P, and the nominal stress is defined as $\sigma_N=P/bD$, where $b=1=$thickness in the third dimension. Expressing the resultant by an integral along the circle from the symmetry line to the notch face, we have $\sigma_N=K_\gamma D^{\lambda-1}\psi(\gamma)$. This gives

$$K_\gamma = \sigma_N D^{1-\lambda}/\psi(\gamma) \tag{13}$$

where

$$\psi(\gamma) = \int_0^{\pi-\gamma} [f_{rr}(\theta,\gamma)\sin\theta + f_{r\theta}(\theta,\gamma)\cos\theta]\,d\theta \tag{14}$$

Note that $\sigma_N=$function of not only K_γ but also of $\psi(\gamma)$ (this shows that the previous investigators' use of K_γ as a criterion for the onset of failure is insufficient). For the limit case of a crack ($\gamma=0$), the resultant may also be obtained from LEFM and is given by $\psi(0)=\sqrt{2/\pi}$.

For notch angles $2\gamma=\pi/3$, $\pi/2$, $2\pi/3$, $5\pi/6$, $89\pi/90$, the solutions of the transcendental equation for λ are 0.5, 0.5122, 0.5445, 0.6157, 0.7520, 0.9783, respectively, and the corresponding $\psi(\gamma)$ values are 0.7979, 0.6762, 0.5836, 0.5156, 0.4916, 0.5263.

To verify the finite-element mode, consider that D is 100 times greater than the length of the FPZ, $2c_f$. The value of c_f can be identified from finite-element results by fitting Bažant's (1984) size effect law to the data for the limit case of a crack ($\gamma=0$). When $D \gg c_f$, the angular distribution of stresses along each circle with $r \geq 0.1D$ ought to match Williams' functions f_{rr}, $f_{r\theta}$, $f_{\theta\theta}$, with negligible deviations. Indeed, the plots of numerical results obtained could not be visually distinguished from these functions; see Fig. 2 (right). Furthermore, as required by Williams' solution, the logarithmic plots of the calculated stress versus r for any fixed θ (and any fixed γ) ought to be straight lines of slope $\lambda-1$, and indeed the finite-element solutions are found to match these straight lines perfectly.

Eqs. (10), (13), and (14) yield the following expression for the nominal strength of the symmetrically loaded notched body for $\theta=0$:

$$\sigma_N = (r/D)^{1-\lambda}\sigma_{\theta\theta}\psi(\gamma)/f_{\theta\theta}(0,\gamma) \tag{15}$$

To determine the effect of notch angle on σ_N, we may proceed similarly to the way nonlinear cohesive fracture is approximated by LEFM. So we assume that, for large enough bodies, a good approximation will be obtained if the value of $\sigma_{\theta\theta}$ calculated from Williams' elastic solution for the point $r=c_f$ (i.e., for the middle of FPZ) is set equal to the material tensile strength, f_t'. This criterion, identical to the criterion proposed for cracks in brittle materials by McClintock (1958), yields

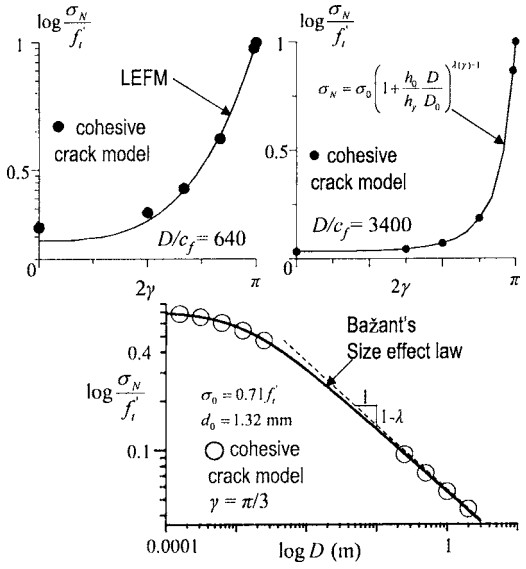

Fig. 3. (Top left) Computed variation of nominal stress with notch angle; (top right) nominal stress obtained by finite-element computations, compared to Eq. (19) for various angles; and (bottom) analytical size effect law for angular notches compared to cohesive crack model

$$\sigma_N = f_t' h(\gamma)(c_f/D)^{1-\lambda(\gamma)} \tag{16}$$

where

$$h(\gamma) = \psi(\gamma)/f_{\theta\theta}(0,\gamma) \tag{17}$$

where $h(\gamma)$=dimensionless function characterizing interaction of a cohesive crack with the near-tip elastic stress field at notch of angle γ. Substituting Eq. (17) into Eq. (13), one gets the large-size angular dependence of the critical stress intensity factor

$$K_{\gamma_{cr}} = f_t' c_f^{1-\lambda(\gamma)}/f_{\theta\theta}(0,\gamma) \tag{18}$$

To verify Eq. (16) for σ_N, geometrically similar scaled circular bodies of different sizes D [Fig. 2 (left)] are analyzed by finite elements for various angles γ. The numerically obtained values of $\log \sigma_N$ for fixed D/c_f are plotted as a function of angle γ; see the data points on the left of Fig. 3, which are seen to match perfectly the analytical solution given by Eqs. (16) and (17) for $D/c_f > 300$. This confirms that the approximation by an equivalent Williams' solution, calibrated by matching the material strength at $r=c_f$, is good enough for any angle and any size $D \geq 300c_f$.

The foregoing expression for $h(\gamma)$ is asymptotically exact for $D/c_f \to \infty$. According to Eq. (16), $h(\gamma)=\sigma_N(D/c_f)^{1-\lambda(\gamma)}/f_t'$, and this expression may be used to calculate from the finite-element results for σ_N the accurate values of function $h(\gamma)$ for various finite values of D/c_f; see Table 1, when the last line indicates the asymptotic values according to Eq. (17). These values can be seen to have errors $<5\%$ if $D/c_f \geq 300$, which is good enough for most engineering purposes.

Size Effect Law for Quasibrittle Structure with V-Notch

A general approximate formula for the effect of structure size D on the nominal strength σ_N of geometrically similar structures with a deep notch of any angle (Bažant and Yu 2004) may now be formulated as follows:

$$\sigma_N = \sigma_0\left(1 + \frac{D}{D_{0\gamma}}\right)^{\lambda(\gamma)-1}, \quad D_{0\gamma} = D_0\frac{h(\gamma)}{h_0} \tag{19}$$

where $h_0=\psi(0)/f_{\theta\theta}(0,0)$=value of $h(\gamma)$ for $\gamma=0$; D_0=transitional size of the size effect for a crack ($\gamma=0$); and $D_{0\gamma}$=transitional size for a notch of angle γ. As we see, the difference from the size effect law for large cracks is that the exponent and the transitional size become functions of notch angle.

Eq. (19) has been derived by asymptotic matching (Bažant 2004) of the following four asymptotic conditions:

1. For $\gamma \to 0$, the classical size effect law $\sigma_N=\sigma_0(1+D/D_0)^{-1/2}$ must be recovered;
2. For $D/l_0 \to 0$, there must be no size effect;
3. For $\gamma=\pi/2$ (smooth surface), size effect of this type must vanish [consideration of size effect of another type (Type 1) occurring at crack initiation from smooth surface is postponed]; and
4. For $D/l_0 \to \infty$, Eqs. (16) and (19) must have an identical form [although numerically the limit of Eq. (19) may slightly differ since it is fitted to different data].

A fifth asymptotic condition, enforcing plasticity-based angular dependence of parameter σ_0, will be imposed later.

Parameter σ_0 in Eq. (19) can be identified in two ways:

1. One way is to match the limit case of a crack ($\gamma \to 0$) by the first two terms of the large-size asymptotic expansion of σ_N in terms of powers of $1/D$, obtained from equivalent LEFM (Bažant and Kazemi 1990; Bažant 2002; Bažant and Planas 1998); this gives

$$D_0 = c_f g'(\alpha_0)/g(\alpha_0), \quad \sigma_0 = \sqrt{E' G_f/c_f g'(\alpha_0)} \tag{20}$$

   where $\alpha=a/D$; a=crack depth; $\alpha_0=\alpha$ value for the initial crack or notch; G_f=fracture energy of the material; $E'=E$=Young's modulus for plane stress; $E'=E/(1-\nu^2)$ for plane strain; $g(\alpha)=k^2(\alpha)$=dimensionless energy release function of LEFM; $g'(\alpha)=dg(\alpha)/d\alpha$; $k(\alpha)=K_I\sqrt{D}/P$; K_I=stress intensity factor; and P=load resultant per unit width. Eq. (20) for D_0, based on the large-size LEFM asymptote for the limit case of a crack, may be retained, as an approximation, for all angles.
2. Another way is to match σ_0 to the asymptotic values of σ_N for $D \to \infty$ and $D \to 0$, ignoring the second terms of the asymptotic expansions in terms of $1/D$ and D. The large-size match is possible only for the case of a crack ($\gamma \to 0$), but the small-size match is possible for all notch angles γ. For the limit of infinitely small beam ($D \to 0$), the cohesive crack model implies that the entire ligament behaves as a crack filled by a perfectly plastic glue (Bažant 2002), with tensile

Table 1. Values of Dimensionless Function $h(\gamma)$ for Various Angles γ and Various Dimensionless Structure Sizes D/c_f, Computed by Finite Elements

	$h(\gamma=0)$	$h(\gamma=\pi/4)$	$h(\gamma=\pi/3)$	$h(\gamma=5\pi/12)$
D/c_f=3,400	2.02	1.86	1.64	1.32
D/c_f=1,700	2.02	1.86	1.65	1.30
D/c_f=340	1.95	1.79	1.57	1.28
D/c_f=17	1.6	1.49	1.40	1.14
$\psi(\gamma)/f_{00}(0,\gamma)$	2.0	1.84	1.62	1.33

yield limit f_t', and the same must logically be expected for any γ. So, at maximum load, there is a uniform tensile stress, $\sigma=f_t'$, across the whole ligament. This stress distribution must be balanced by a concentrated compressive force, $b(D-a)f_t'$, at the top face of beam (because the cohesive crack model has no bound on compressive stress). For a structure of given geometry, the equilibrium condition on the ligament cross section yields the corresponding σ_N; e.g., for the special case of a three-point-bend test beam of depth D and span L, with a notch of depth a, one thus gets, regardless of notch angle

$$\sigma_0 = 2(1-a/D)^2 f_t' D/L \tag{21}$$

The former type of calibration has worked better for size effect in quasibrittle structures with large cracks, in which the response is usually closer to the LEFM asymptote than the horizontal plastic asymptote. But for large-angle notches, for which the limit case of equivalent LEFM for a crack is remote, the latter type of calibration may be more realistic.

Ideally, one should match the first two terms of both the small- and large-size asymptotic expansions for the limit case of a crack. But this would require a more complex formula with four free parameters. Such a formula was presented in Bažant et al. (2002) for the limit case of a crack.

Substituting Eq. (19) into Eq. (13), and noting that $k(0)=\sqrt{g(\alpha_0)}$, one can alternatively express the size effect law in terms of the critical generalized stress intensity factor (or notch toughness)

$$K_{\gamma_{cr}} = \sigma_0 D^{1-\lambda(\gamma)} k(\gamma)\left(1+\frac{D}{D_{0\gamma}}\right)^{\lambda(\gamma)-1}, \quad k(\gamma)=\frac{1}{\psi(\lambda)} \tag{22}$$

For $\gamma\to 0$, the use of Eq. (20) shows that this expression reduces to the well known (Bažant 2002) size effect law for large cracks in terms of the apparent critical stress intensity factor

$$K_{cr} = K_{Ic}\sqrt{\frac{D}{D+D_0}} \quad \text{for } \gamma\to 0 \tag{23}$$

where $K_{Ic}=\sqrt{E'G_f}=\sigma_0\sqrt{D_0 g(\alpha_0)}$.

Comparisons with Cohesive Crack Simulations and Size Effect Experiments

As an example, the parameters $f_t'=58.0$ MPa and $G_f=77.3$ N/m are considered for the linear stress-separation diagram of cohesive crack. Also $E=42.56$ GPa and $\nu=0.36$. The size-effect plot of log σ_N versus log D for one notch angle, $\gamma=\pi/3$, according to Eq. (19) is compared in Fig. 3 (bottom) to the data points obtained by finite-element predictions for notched circular bodies with cohesive crack (crack lengths from 0.01 to 0.8D are considered). The agreement is seen to be good.

The notch angle effect is compared on the right of Fig. 3, which shows by data points the σ_N values computed by finite elements for angles $\gamma=0$, $\pi/4$, $\pi/3$, $5\pi/12$, $89\pi/90$, and π, all for only one size $D=0.5$ m. The agreement is again good.

The most comprehensive experimental data to fit are those of Dunn et al. (1997). These investigators used plexiglass [i.e., polymethyl methacrylate (PMMA)—an isotropic amorphous glassy thermoplastic polymer which is homogeneous, at normal scales of usage, and brittle near room temperature]. They tested three-point-bend beams (Fig. 4), seeking to determine the relation between the nominal strength and the critical

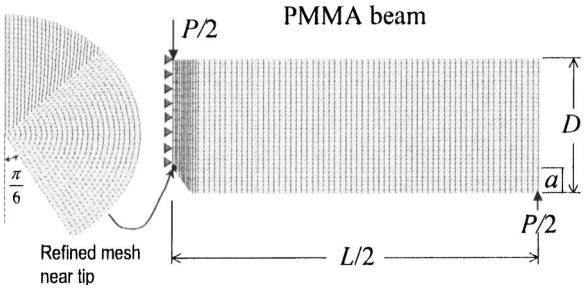

Fig. 4. Notched three-point bend beams tested by Dunn et al. (1997), and mesh used in finite-element analysis

K_γ. In all tests, beam depth $D=17.8$ mm, specimen thickness $b=12.7$ mm, beam span $L=76.2$ mm, Young's modulus $E=2.3$ GPa, and Poisson's ratio $\nu=0.36$. Tests were made for three notch angles, $2\gamma=\pi/3,\pi/2,2\pi/3$, with four notch-depth ratios $a/D=0.1,0.2,0.3,0.4$ for each angle (a=length of orthogonal projection of notch face onto the notch symmetry line).

In Dunn's tests, there are four specimens for each $2\gamma=\pi/3$ and $2\pi/3$, and three specimens for each $2\gamma=\pi/2$. For different a/D, the σ_0 and D_0 values are not the same as in Eq. (19). To identify them from tests, Eq. (19) may be transformed as

$$Y = \frac{A}{B(\alpha)}\left[1+C\frac{g_0(\alpha)}{h_\gamma B^2(\alpha)}\right]^{\lambda-1} \tag{24}$$

where $\alpha=\alpha/D$; $Y=\sigma_N$; $A=f_t'$=tensile strength; $C=Dh_0A^2/K_{Ic}^2$; and $B(\alpha)=L/2(1-\alpha)^2D$ according to Eq. (21). Because λ is variable, this cannot be transformed to a linear regression plot, but constants A and C in Eq. (24) can be identified by minimizing the sum or errors in Y with the help of a standard library subroutine for the Levenberg–Marquardt nonlinear optimization algorithm.

Fig. 5 (bottom) shows four plots of σ_N versus 2γ, in which the predictions of Eq. (24) with optimum A and C are compared to the data points from Dunn et al.'s tests, for each a/D. The predictions are seen to be quite close. The coefficient of variation ω_i of the errors in Y (defined as the square root of the mean of the squares of errors, divided by the mean of all data points in the plot) is stated in each of the 4 plots for various a/D ($i=1,\ldots,4$). The combined coefficient of variation for all the data points, $\omega=[(\Sigma_i\omega_i^2)/n]^{1/2}=4.4\%$, which is satisfactory.

From the optimal value of A and C, one can get f_t', then the critical stress intensity factor, K_{Ic} (i.e., fracture toughness), and finally G_f. The optimized $f_t'=54.7$ MPa; this is close to the result of uniaxial tensile tests conducted by Dunn et al., which is $\sigma_y=51$ MPa. The optimal K_{Ic} is 1.26 MPa$\sqrt{\text{m}}$, while Dunn et al.'s standard fracture toughness test gave 1.02 MPa$\sqrt{\text{m}}$, with the standard deviation of 0.12 MPa$\sqrt{\text{m}}$ (the difference may be due to an error in the effective crack length estimated from the unloading stiffness).

The plexiglass tests have also been simulated by finite elements, using meshes exemplified in Fig. 4 for notch angle $2\gamma=\pi/3$ and notch-depth ratio $a/D=0.2$. The mesh was gradually refined toward the notch tip but the first 60 rings of elements had the same width $h=R/3{,}600$ where $R=D-a$=ligament length. Because plexiglass exhibits some degree of ductility, the softening stress–separation curve of the cohesive crack model was assumed as rectangular, with height f_t' and area of the rectangle equal to G_f. Fig. 5 (bottom) shows a comparison of the finite-

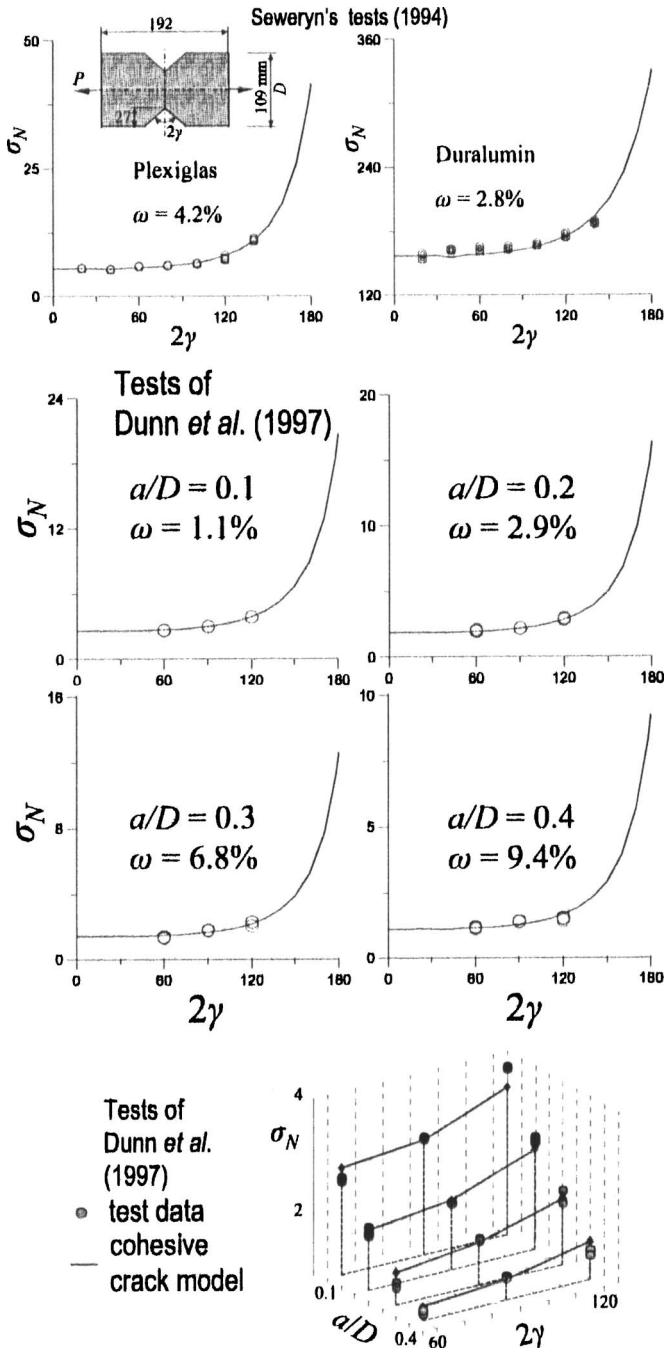

Fig. 5. (Top row) Seweryn's (1994) test data on effect of notch angle on nominal strength of DENT specimens, and their fits by proposed formula for angular size effect; (lower rows) computed nominal stress for different notch angles γ and different notch depths a/D, compared to Dunn et al.'s (1997) test results

element results (solid lines) with the experiments (solid circles). The differences are seen to be small. The coefficient of variation of the deviations from data points is $\omega=6.9\%$ (root-mean-square error divided by the mean of all data).

V-notch tests on PMMA have also been reported by Carpinteri (1987). These tests are not analyzed here, because of missing information on f_t' and K_{Ic}.

Seweryn (1994) reported tests of double-edge-notched tension specimens, one set made of plexiglass, and another of duralumin (aluminum alloy with 4% copper and traces of manganese, magnesium, and silicon) [Fig. 5 (top)]. For each material, specimens with eight notch angles, varying from 20° to 160°, with an interval of 20°, were tested. With the help of the Levenberg–Marquardt optimization algorithm, these test data are fitted by Eq. (19) rearranged as follows:

$$Y = A(1 + C/h_\gamma)^{\lambda-1} \tag{25}$$

where

$$Y = \sigma_N, \quad A = \sigma_0, \quad C = Dh_0/D_0 \tag{26}$$

However, the test data for notch angle $2\gamma=160°$ must be excluded from the fitting by Eq. (19) because they probably lie outside the range of applicability of the present solution based on Williams' singular stress field. The reason is that the present size effect formulation captures only the size effect due to large cracks or notches (Type 2 size effect), but not the size effect at crack initiation [called Type 1 size effect, Bažant (2002, 2004)], resulting from stress redistribution caused by the boundary layer of cracking; see a later section on Type 1 size effect occurring for $2\gamma=\pi$, for which Eq. (19) gives no size effect. For angles less than π, probably including 160°, there must be a continuous transition from Type 2 to Type 1 size effect, not captured by Eq. (19).

Seweryn's test results are shown by the data points in the plot of σ_N versus 2γ in Fig. 5 where plexiglass (methyl methacrylate) is on the left, and duralumin on the right. For comparison, the figure also shows, as the solid line, the least-square fit of the data points by Eq. (19). The vertical deviations of the data points from the optimum fit have the coefficient of variation of $\omega=4.2\%$ for plexiglass and $\omega=2.8\%$ for duralumin.

Eq. (19) may further be justified by comparing the values of critical stress intensity factor K_{Ic}. The foregoing optimization of data fit yields the value of C in Eq. (25), from which one can calculate the transitional size for a crack, $D_0=h_0D/C$, where D=characteristic size of the specimen as shown in Fig. 5. According to Eq. (20), $K_I=\sigma_0\sqrt{D_0 g_0}$, where, for the geometry used, g_0 can be easily obtained from a handbook (e.g., Tada et al. 1985). Thus one gets $K_{Ic}=1.82\ \text{MPa}\sqrt{\text{m}}$ for plexiglass, and $K_I=60.2\ \text{MPa}\sqrt{\text{m}}$ for duralumin. Standard fracture toughness tests by the author gave 1.79 and 56 $\text{MPa}\sqrt{\text{m}}$, respectively. On the other hand, the general definition $K_{Ic}=\sigma_N\sqrt{g_0 D}$ for a crack can be used to determine the stress intensity factor after calculation of σ_N according to Eq. (19) for $2\gamma=0$. This yields $K_{Ic}=1.81$ and 53.1 $\text{MPa}\sqrt{\text{m}}$, respectively, which differs from the standard fracture toughness test by only 1.9 and 7.1%, respectively.

Type 2 Size Effect and Its Transition to Type 1

In the limit of $\gamma\to 0$, Eq. (19) tends to the size effect for structures with zero-angle notches, called Type 2 size effect (Bažant 2002, 2004). This size effect occurs if the notch is sufficiently deeper than the thickness D_b of the boundary layer of a heterogeneous structure, which is proportional to l_0, and is, for concrete, about two aggregate sizes deep. Therefore, the validity of the proposed size effect law Eq. (19) must be restricted to notches of depth a sufficiently greater than D_b. For concrete, this means notches sufficiently deeper than the maximum aggregate size, d_a. For sharp reentrant corners in normal-size concrete structures, this condition is probably not satisfied, and so such corners probably do not significantly weaken the structure beyond what is calculated for the reduced cross section on the

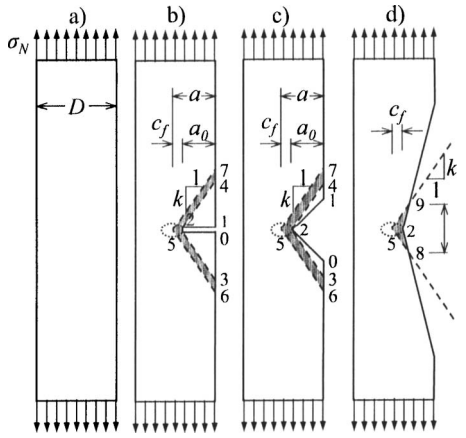

Fig. 6. Intuitive explanation of size effect for crack and for notches of two different angles

basis of material strength. However, for very large concrete structures, the size effect due to sharp reentrant corners cannot be ignored.

A similar size effect occurs in concrete under compression (Bažant and Planas 1998; Bažant 2002), especially for cyclic loading. It might be that the size effect of such a corner in a highly compressed region of concrete was what helped to trigger the collapse of some very large structures, such as the record-span box girder of Koror-Babeldaob Bridge in Palau. A thorough examination of this possibility would not be inappropriate.

As already mentioned, there also exists a size effect of Type 1, which is different and is exhibited by quasibrittle structures failing at crack initiation from a smooth surface. However, this effect disappears for cracks and notches (of any angle) shallower than D_b, for which the singular elastic stress field of a notch is not even approximately approached. For such situations, correct results will be obtained with the classical plastic limit analysis based on material strength, taking into account both the cross section reduction due to notch and the stress redistribution due to distributed cracking near the notch tip, reaching to depth D_b from the tip. The latter, computed in the same way as for the case of a smooth surface (Bažant and Li 1995a,b), will automatically give the Type 1 size effect in the presence of a notch.

Because, for $2\gamma \to \pi$, the size effect formula in Eq. (19) does not continuously approach the Type 1 size effect for failures at crack initiation, the practical applicability of Eq. (19) should be restricted—perhaps to notch angles $\leqslant 3\pi/4$. A generalization will be needed to describe the transition to Type 1 analytically.

To capture a continuous transition from shallow notches to deep notches, and a continuous transition from the Type 1 size effect for shallow cracks to Type 2 size effect for deep cracks (for $\gamma \to 0$), Eq. (19) will have to be amalgamated with the universal size effect law (Bažant 2002, 2004; Bažant and Yu 2006).

Simple Intuitive Explanation

From Figs. 3 and 5, it may be noted that V-notches of angles 2γ up to about 90° behave almost the same as sharp cracks and produce almost the same size effect. This fact may be intuitively explained by a similar argument as that from which the size effect law for large cracks was first derived (Bažant 1984). Consider the specimen in Fig. 6(a), of thickness b, which is initially under uniform tensile stress $\sigma=\sigma_N$. Introducing a crack or cutting a notch $\overline{021}$ at constant end displacements relieves the stress approximately from the triangular lightly shaded regions $\overline{0230}$ and $\overline{1421}$ limited by lines of slope k. This slope is about the same for a crack and a notch of angle less than about 90°, and is approximately independent of specimen size D (the effective value of k of course depends on geometry, and can be determined only by exact elastic stress analysis).

For the crack to propagate [Fig. 6(b)], or a crack to initiate from the notch tip [Fig. 6(c)], a FPZ of a certain fixed length $2c_f$ must develop first. Because of the formation of FPZ, stress is additionally relieved from darkly shaded regions $\overline{25632}$ and $\overline{52475}$, the combined area of which is $2b(ka)c_f$ where $a=a_0+c_f$=length of equivalent LEFM crack. The strain energy released from these regions is $2bkac_f(\sigma_N^2/2E')$. According to equivalent LEFM, this must be equal to the energy consumed and dissipated by crack increment $\triangle a=c_f$, which is bc_fG_f. Solving σ_N from this equality, one gets $\sigma_N=\sigma_0(1+D/D_0)^{-1/2}$, where $D_0=c_fD/g_0$, $\sigma_0=(E'G_f/kc_f)^{1/2}$. If geometrically similar specimens and cracks are considered, then D/a_0=constant, and so both D_0 and σ_0 are constant. Therefore, by this simplified argument, one obtains the same σ_N and the same size effect law for both the crack and the notch in Figs. 6(b and c).

The simple reason why there is a size effect is that the energy release caused by crack increment c_f is proportional to σ_N^2ka, whereas the dissipated energy, which must be equal, is proportional to G_f, and thus constant. Since a increases with D, σ_N must decrease in order to keep σ_N^2a constant.

If the notch angle is too large, as shown in Fig. 6(d), then lines $\overline{58}$ and $\overline{59}$ of slope k terminate on the notch face close to the tip, and the darkly shaded stress relief region $\overline{28592}$ becomes small and almost independent of notch depth a_0. The energy release caused by extending the tip of equivalent LEFM crack to point 5 is $(bc_f/2)\sigma_N^2/2E' \times$ distance $\overline{89}$. Since, for large angles, this distance can get much smaller than ka and tends to become independent of a, the size effect (or energy release type) must diminish as the notch angle becomes large.

Conclusions

1. A physically realistic approach to predicting the effect of a sharp reentrant corner or notch on the structural strength is to consider a cohesive crack to propagate from the notch tip.
2. The basic hypothesis of analysis, verified both experimentally and computationally, is that the V-notch near-tip elastic field provides a good global approximation to the nonlinear solution for the cohesive crack model if the material tensile strength is equated to the stress value in the near-tip elastic field at some fixed distance from the tip. This distance is independent of the notch angle and proportional to Irwin's characteristic length of the fracture process zone. This hypothesis leads to a formula for the effect of notch angle on the nominal strength of very large brittle structures. Alternatively, this formula can be expressed in terms the critical value of the generalized V-notch stress intensity factor.
3. A simple size effect law for nominal strength of V-notched structures is derived by asymptotic matching of five limit cases: (1) Bažant's size effect law for quasibrittle structures with large cracks when the notch angle approaches zero; (2) absence of size effect when the structure size tends to zero;

(3) absence of size effect (of Type 2) when the notch angle approaches π; (4) the notch angle effect for plastic limit analysis based on material strength when the structure size tends to zero; and (5) the aforementioned formula for the notch angle effect on crack initiation in brittle structures when the structure size tends to infinity. An equivalent formula is also derived for the angle and size dependence of the critical generalized V-notch stress intensity factor.

4. The proposed size-and-angle effect law is verified by two kinds of finite-element simulation of V-notch with cohesive crack: (1) for a circular body, chosen for its convenience in simulating the full range of notch angles; and (2) for a three-point-bend beam with the V-notch.
5. The proposed law is also verified by experimental data of Dunn et al. (1997) for three-point-bend plexiglass (PMMA) beams in which both the notch depth ratio and notch angle were varied, and Seweryn's (1994) test data for double-edge-notched tension specimens made of plexiglass and duralumin, in which only the notch angles were varied.
6. The nonlinear fracture parameters in the size effect law can be numerically calibrated in two ways: (1) by matching the first two terms of the large-size asymptotic power-series expansion of equivalent LEFM; or (2) by matching the fracture energy and material strength (or material characteristic length) according to the cohesive crack model. While the former has worked well for large concrete structures, the latter is found to give better predictions for the three-point-bend experiments due to their small size.
7. The present formulation belongs to Type 2 size effect as previously classified for cracks. It is not applicable for notches not deeper than the boundary layer of cracking, the thickness of which is 1–2 maximum aggregate sizes in concrete. The transition to size effect for notch angles close to 180° is also not described.

Acknowledgments

The basic theory was supported under ONR Grant No. N00014-10-I-0622 to Northwestern University (from the program directed by Yapa D. S. Rajapakse), and the numerical studies were supported under a grant from the Infrastucture Technology Institute of Northwestern University.

References

Barenblatt, G. I. (1962). "The mathematical theory of equilibrium cracks in brittle fracture." *Adv. Appl. Mech.*, 7, 55–129.

Bažant, Z. P. (1984). "Size effect in blunt fracture: Concrete, rock, metal." *J. Eng. Mech.*, ASCE, 110(4), 518–535.

Bažant, Z. P. (2002). *Scaling of structural strength*, Hermes Penton Science (Kogan Page Science), London; also updated French translation, Hermes, Paris, 2004; and 2nd Ed., Elsevier, London, 2005.

Bažant, Z. P. (2004). "Scaling theory for quasibrittle structural failure," *Proc. Natl. Acad. Sci. U.S.A.*, 101(37), 13397–13399.

Bažant, Z. P., and Estenssoro, L. P. (1979). "Surface singularity and crack propagation." *Int. J. Solids Struct.*, 15, 405–426.

Bažant, Z. P., and Kazemi, M. T. (1990). "Determination of fracture energy, process zone length and brittleness number from size effect, with application to rock and concrete." *Int. J. Fract.*, 44, 111–131.

Bažant, Z. P., and Li, Y.-N. (1995a). "Stability of cohesive crack model: Part II—Eigenvalue analysis of size effect on strength and ductility of structures." *J. Appl. Mech.*, 62, 965–969.

Bažant, Z. P., and Li, Z. (1995b). "Modulus of rupture: Size effect due to fracture initiation in boundary layer." *J. Struct. Eng.*, 121(4), 739–746.

Bažant, Z. P., and Planas, J. (1998). *Fracture and size effect in concrete and other quasibrittle materials*, CRC, Boca Raton, Fla.

Bažant, Z. P., and Yu, Q. (2004). "Size effect in concrete specimens and structures: New problems and progress." *Fracture Mechanics of Concrete Structures, Proc., FraMCoS-5, 5th Int. Conf. on Fracture Mechanics of Concrete and Concrete Structures*, Vail, Colo., V. C. Li, K. Y. Leung, K. J. Willam, and S. L. Billington, eds., Vol. 1, 153–162.

Bažant, Z. P., and Yu, Q. (2006). "Universal size effect law and effect of crack depth on quasibrittle structure strength." *Rep.*, Northwestern Univ., Evanston, Ill.

Bažant, Z. P., Yu, Q., and Zi, G. (2002). "Choice of standard fracture test for concrete and its statistical evaluation." *Int. J. Fract.*, 118(4), 303–337.

Brahtz, J. H. A. (1933). "Stress distribution in a reentrant corner." *Trans. ASME*, 55, 31–37.

Carpinteri, A. (1987). "Stress-singularity and generalized fracture toughness at the vertex of re-entrant corners." *Eng. Fract. Mech.*, 26, 143–155.

Dunn, M. L., Suwito, W., and Cunningham, S. J. (1996). "Stress intensities at notch singularities." *Eng. Fract. Mech.*, 34(29), 3873–3883.

Dunn, M. L., Suwito, W., and Cunningham, S. J. (1997). "Fracture initiation at sharp notches: Correlation using critical stress intensities." *Int. J. Solids Struct.*, 34(29), 3873–3883.

England, A. H. (1971). "On stress singularities in linear elasticity." *Int. J. Eng. Sci.*, 9, 571–585.

Gómez, F. J., and Elices, M. (2003). "A fracture criterion for sharp V-notched samples." *Int. J. Fract.*, 123(3–4), 163–175.

Griffith, A. A. (1920). "The phenomena of rupture and flow in solids." *Philos. Trans. R. Soc. London, Ser. A*, 221, 163–198.

Hillerborg, A., Modéer, M., and Petersson, P. E. (1976). "Analysis of crack formation and crack growth, in concrete by means of fracture mechanics and finite elements." *Cem. Concr. Res.*, 6, 773–782.

Hussain, M. A., Pu, S. L., and Underwood, J. (1974). "Strain energy release rate for a crack under combined Mode I and II." *ASTM Spec. Tech. Publ.*, 560, 2–28.

Irwin, G. (1958). "Fracture." *Handbuch der Physik*, W. Flügge, ed., Vol. 6, Springer, Berlin, 551–590.

Kalandiia, A. I. (1969). "Remarks on the singularity of elastic solutions near corners." *Prikl. Mat. Mekh.*, 33, 132–135.

Karp, S. N., and Karal, F. C. J. (1962). "The elastic-field behavior in the neighborhood of a crack of arbitrary angle." *Commun. Pure Appl. Math.*, 15, 413–421.

Knein, M. (1926). "Zur Theorie des Druckversuchs." *Z. Angew. Math. Mech.*, 6, 414–416.

Knein, M. (1927). "Zur Theorie des Druckversuchs." *Abhandlungen aus dem aerodynamnischen Institut an der Technischen Hochschule Aachen*, Heft 7, 43–62.

Kosai, M., Kobayashi, A. S., and Ramulu, M. (1993). "Tear straps in airplane fuselage." *Durability of metal aircraft structures*, Atlanta Technology Publishers, Atlanta, 443–457.

McClintock, F. A. (1958). "Ductile fracture instability in shear." *J. Appl. Mech.*, 25, 582–588.

Novožilov, V. V. (1969). "On necessary and sufficient criterion of brittle fracture." *Prikl. Mat. Mekh.*, 33, 212–222.

Palaniswamy, K., and Kuauss, E. G. (1972). "Propagation of a crack under general in-plane tension." *Int. J. Fract. Mech.*, 8, 114–117.

Rice, J. R. (1968). "Mathematical analysis in the mechanics of fracture." *Fracture—An advanced treatise*, H. Liebowitz, ed., Vol. 2, Academic, New York, 191–308.

Ritchie, R. O., Knott, J. F., and Rice, J. R. (1973). "On the relation between critical tensile stress and fracture toughness in mild steel." *J. Mech. Phys. Solids*, 21, 395-410.

Seweryn, A. (1994). "Brittle fracture criterion for structures with sharp notches." *Eng. Fract. Mech.*, 47, 673–681.

Seweryn, A., and Mróz, Z. (1995). "A non-local stress failure condition

for structural elements under multiaxial loading." *Eng. Fract. Mech.*, 51, 955–973.

Tada, H., Paris, P. C., and Irwin, G. R. (1985). *The stress analysis of cracks handbook*, Paris Productions, Saint Louis.

Wang, T. C. (1978). "Fracture criteria for combined mode cracks." *Sci. Sin.*, 21, 457–474.

Williams, M. L. (1952). "Stress singularities resulting from various boundary conditions in angular corners of plates in extension." *J. Appl. Mech.*, 74, 526–528.

Zi, G., and Bažant, Z. P. (2003). "Eigenvalue method for computing size effect of cohesive cracks with residual stress, with application to kink bands in composites." *Int. J. Eng. Sci.*, 41(13–14), 1519–1534.